European Annals of Dental Sciences
Official Publication of Ankara University, Faculty of Dentistry

EADS, 2022, 49 (3), 131–138

e-ISSN : 2757-6744
doi : 10.52037/eads.2022.0040

Article Received/Accepted : October, 16 2022 / November, 10 2022

ORIGINAL RESEARCH ARTICLE

Comparison of the Effect of the Time Under the Three Primary Color Lighting of LED Production Before Scanning of Phosphorus Plates

Hakan Amasya [1*], Kaan Orhan [2] and Afra Alkan [3]

[1]Department of Dentomaxillofacial Radiology, Faculty of Dentistry, İstanbul University-Cerrahpaşa, İstanbul, Turkey and [2]Department of Dentomaxillofacial Radiology, Faculty of Dentistry, Ankara University, Ankara, Turkey and [3]Department of Biostatistics and Medical Informatics, Ankara Yildirim Beyazit University, Ankara, Turkey

*Corresponding Author; h-amasya@hotmail.com

Abstract

Purpose: This study aimed to compare the effect of light exposure in red, green and blue (RGB) colors prior to scanning of the PSP plates.
Materials and Methods: An Arduino-based embedded system was produced for standardized light exposure to the irradiated PSP plates. The system consisted of an Arduino Mega 2560 developer board, 2 RGB LED light sources, a TSL2591 digital light sensor and a DHT11 temperature and humidity sensor. A light-tight platform was produced with additive manufacturing and electronical units were integrated into this platform. A two-step alloy was used to create contrast. PSP system (VistaScan, Dürr Dental, Germany) was irradiated with fixed parameters of 70 kV, 8 mA and 0.5 seconds. Scanning of the PSPs were delayed for 1-, 3-, 5-, and 10-minutes, and half of the active surfaces were exposed to RGB lights independently in full brightness (PWM) and calibrated with LUX, while the rest was protected. MGVs were measured in six regions per image. The MGV differences in regions between conditions were examined by Kruskal-Wallis test. A p-value<0.05 was considered statistically significant.
Results: In PWM setup, signal loss was higher in blue color at 1-, 3-, and 5-minutes, but at 10-minutes, only the green light produced half-image. In LUX setup, signal loss was lower in green light. Contrast loss was lower in green light with LUX calibration (p<0.05).
Conclusions: Among the three LED colors compared, effect of exposure to green light prior to scanning of the irradiated PSP plates was found to be lower than the blue and red colors.

Key words: Digital radiology; Material science; Photostimulable phosphor plate

Introduction

Analog films in conventional intraoral radiography contains silver halide particles dispersed in a gelatin matrix. X-rays reaching the film sensitize the initial state of the silver halide particles, and non-irradiated particles are fixed in the gelatin matrix while the rest is washed away by a chemical process. As a result, the fixed particles reduce the light transmittance of the film, hence black and white regions can be produced in the resulting radiograph depending on the x-ray exposure.[1,2] Once the exposure is over, the geometry of the attenuated x-rays is already stored in the film; however, this 'latent image' cannot be discerned by the eye until the film is developed under proper conditions. Analog films are sensitive to visible light before chemical treatment and are provided in an opaque sheath. The film development process should be completed without delay. Due to the sensitivity to ambient light, applications such as the use of dim red light and coin testing are adopted in the conventional film development procedures.[2]

In conventional radiography, a single disposable analog film can be used for both capturing the radiation and displaying the image.[1] In contrast, digital sensors are re-usable and digital radiographs are displayed on monitors. Digital sensor technologies in intra-oral imaging can be categorized as solid-state (SS) sensors and phosphor storage plates (PSPs).[1,3] In SS systems, x-rays can be converted into an electrical signal without any conversion, or the radiation can be converted into light by a scintillator first and then the light is captured to produce the electrical signal, simultaneously. Charge-coupled device (CCD) and complementary

How to cite: Amasya H., Orhan K., Alkan A. Comparison of the Effect of the Time Under the Three Primary Color Lighting of LED Production Before Scanning of Phosphorus Plates. EADS. 2022;49(3):131-140

metal-oxide-semiconductor (CMOS) detectors convert the light into electrons and are used in both digital cameras and dental radiography systems.[3,4] However, in digital cameras, it is essential to capture the ambient light for image production, while in dental radiography, the interest is restricted to capturing the light converted from x-rays using a scintillator.[1] SS sensors in dental radiography are secured in a liquid- and light-proof container; hence the effect of the ambient light can be neglected. The produced signal is digitized by an analog-digital converter and transferred directly to the computer.[3,4]

PSP images are produced by scanning the digital sensor with a laser scanner after radiation exposure, and the technology is based on the phenomenon called photostimulated luminescence (PSL). Some crystals, such as alkali halides, can store the energy of ionizing radiation for a period of time, and a luminescence may occur after stimulation with a proper light in the PSL stimulation spectrum.[5,6] The mechanism of PSL suggested by a trap model, which depends on the presence of electron/hole traps. Exposure of crystals to ionizing radiation traps some electrons in the F-centers or hole-trapped centers, and de-trapping of the electrons require energy. Stimulating light in a wavelength within the F-band absorption spectrum releases some of the trapped electrons, resulting in an emission defined as PSL. Moreover, doping the alkali halides with Eu^{2+} enhances the PSL properties of the material.[5,7] PSPs consist of a polymer base coated with europium-activated alkali halide emulsion. BaFBr:Eu^{2+} is a common phosphor compound used in medical imaging, and an Argon ion laser (514 nm), a frequency doubled YAG:Nd^{3+} laser (532 nm) or a He-Ne laser (633 nm) can be used in the scanner.[5,6] Irradiated PSP plates are stimulated by laser according to the coordinates consisting of rows and columns, and the resulting PSL is converted into electrical signal by a photomultiplier tube.[5] The laser light used in the scanner to stimulate the PSP is filtered out for more precise recording of the PSL. The electrical signals produced by scanning of the PSP surface are digitized by the analog-digital converter. The data obtained in the scanning process is transferred to the computer to produce the image. The remaining information on the PSP is erased by applying an intense light and the sensor is prepared to be used on a new patient inside a hygienic plastic cover.[4–6]

Microcontrollers are embedded systems in which a central processing unit (CPU) and peripheral units are supported by a software, to perform one or a few tasks at a minimum cost. On the other hand, microprocessors (a.k.a. the CPUs) are developed as stand-alone rather than integrated with peripherals and are supported by externals for various tasks. The difference between a microcontroller and microprocessor is that the first is dedicated for a single task, while the latter is much faster, but production cost is higher.[8] It is essential to keep the production cost and energy consumption to a minimum while getting the task done. Arduino is an open-source electronics platform based on easy-to-use hardware and software. The Arduino project was first developed in Italy in 2005.[9,10] The development boards are designed to be used by teachers, students, and hobbyists, in executing their dream prototypes. Therefore, simplicity and ease of use are at the forefront.[8,9] Various input or output units compatible with the system can be connected without any soldering, from analog or digital pins on the board, or with connection protocols such as I2C or USB. The system can be coded using a basic syntax similar to the C and the simplified C++, and executable programs can be developed via Arduino Integrated Development Environment (IDE). Arduino exists in many variants. such as Uno, Nano, and Mega, and key factors for choosing the convenient board are its physical dimensions. processor and CPU power, I/O capability, voltage, memory size and project design. Several input units like sensors or buttons and output units like motors or lights are available to be used with the Arduino boards.[8,9] While developing an Arduino system, the most suitable hardware for the task should be considered, and a software should be designed with care to make effective use of the hardware. Three-dimensional (3D) printing, also known as additive manufacturing (AM), is a method in which a 3D object is produced by adding successive layers of material under computerized control.[11,12] While the material is milled in production with the milling technique, in AM, the product is generated from the bottom to the top.[13] The freedom to manufacture custom-made medical products and equipment provides a great advantage for medical purposes, and its use in the field of dentistry expand every day.[11] The first step in making a custom fabrication for a patient is to acquire the virtual patient, and for this, alternatives such as digital volumetric radiological data or optical scan data of the patient can be merged. Customized jigs, fixtures, implants, and tools can be designed with various 3D modelling software, and the digital design can be produced with technologies such as digital light processing, selective laser melting, fuse deposition modeling, and stereolithography, etc.[11,12] The principle, structure, advantages and disadvantages of each technology are the criteria that determine the most suitable technique for the final product.[11] Although 3D manufacturing is of interest to healthcare professionals, its fundamental use is rapid prototyping. A platform suitable for a project involving electromechanical circuits can be produced with the AM technique.[14,15]

In SS systems, the image is produced directly without the need for film development or any scanning procedure. Unlike SS sensors, conventional and PSP imaging requires chemical processing or scanning procedures after the radiation exposure to reveal the 'latent image'.[2,3] It is essential to keep the analog film away from the environment light until the chemical development is completed, however, the storage PSPs can be operated in the day-light conditions. Still, electrons stored in the PSP plate are continually released over time.[16] In 2005, Akdeniz et al. tested longevity of image quality in storage phosphor plates (SPPs) at various exposure settings, storage conditions, and delays in scanning. Fifteen PSP plates were exposed from 0.08 to 0.20 seconds and scanned immediately, 10, 30, and 60 minutes, and 24 hours after exposure. Plates were stored both in daylight and in a light-tight box. Results of the study demonstrated an increase in mean grey values (MGVs) for both storage conditions, however, the MGVs of plates kept in daylight were found to be significantly higher than those stored in a light-tight environment. Also, the authors recommended that the delay time should not exceed 10 minutes after exposure.[17] In 2017, Eskandarloo et al. conducted a study to evaluate the impacts of different combinations of storage conditions and varying delays in reading of digital images captured using PSPs. The plates were re-exposed and stored in four different storage conditions: white light, yellow light, natural light environment, and dark room; then scanned after 10 and 30 minutes and 4 and 8 hours. Authors reported that the resulting images showed a significant decrease in the density of plates scanned after 10 minutes or longer from the exposure. Moreover, the yellow light environment had a different impact on the quality of PSP images.[18] This study aimed to compare the effect of red, green, and blue ambient light colors in delayed scanning of the PSP plates, by developing an Arduino-based platform for production of light with a LED source and the calibration of the light intensity using a light sensor.

Material and Methods

This study was conducted in 3 steps. First, an Arduino-based platform was developed for producing the desired ambient light. Then, the radiographic procedures were performed, and digital images were acquired in different light conditions. Lastly, mean MGVs were measured, and statistical analysis was performed.

Development of the Arduino-based Lumination Platform

The system was designed with Arduino Mega 2560 developer board based on ATmega2560 microcontroller at 16 MHz clock speed, 256 KB flash memory, 8 KB SRAM and 4 KB EEPROM. Light, temperature and humidity sensors were used as the input unit, and two RGB LED modules were used as the output unit. TSL 2591 light sensor was used for measuring both infrared and visible light, from 188 uLUX up to 88,000 LUX with 600,000,000:1 dynamic range and connected to I2C bus. DHT11 temperature and humidity sensor was connected using digital pins, to track the temperature in the range of 0°C to 50°C (±1°C) and humidity in the range of 20% to 90% (±1%). All units were connected with jumper wires without the need for soldering. Adafruit libraries of <Wire.h>, <Adafruit_Sensor.h> and "Adafruit_TSL2591.h" (https://github.com/orgs/adafruit/repositories) were used to program the sensors. The light sensor was coded for 'medium gain' and '100 ms integration time'. The developed software was uploaded to the device via the Arduino IDE. Light in red, green, and blue colors was produced by the RGB LED module and the output was adjusted by manipulating pulse width modulation (PWM) values between 0 and 255 dedicated for each color. The system was powered by a USB port and the sensor data was monitored through the serial port screen using a personal computer (Figure 1).

The light-tight platform was designed in 3D as six parts with SolidWorks software. Within the platform, the light sensor was placed on the floor, the LED sources were designed on the ceiling, and the temperature and humidity sensor were fixed on the back wall. The distance between the floor and the ceiling is designed as 10 centimeters. A visor was created on the floor to shield half of the imaging plates from the exposure to the produced light. The designed parts were "exported" in ".STL" format. STL files were prepared with Ultimaker Cura and Creality Slicer slicing programs to be manufactured with Ultimaker S3 and Creality CR10 Smart Pro 3D printers. All parts on the platform were printed in 65 hours using 445 grams of PLA filament. The inner surface of the parts was covered with matte black acrylic paint. Arduino units were fixed to the system after the compatibility of the produced parts was checked and the installation of the platform was completed. The system was calibrated in the dimly lit room where the phosphor plates were scanned. For this, the LEDs were turned on in full cycle (PWM: 255) in each color and the illumination values on the ground were recorded in the LUX unit. Thus, the color with the weakest light output was determined and the PWM values that created similar illumination in other colors were determined. As a result, the development of the Arduino-based platform has been completed (Figure 2).

Proceedings of the PSP Plates

Radiographic images were obtained with 31 x 41 mm phosphor plates (Dürr Dental, Germany) in lightproof hygienic covers. Two cylindrical metal alloys with diameters of 23.85 mm and 20.5 mm were used to create contrast areas in the middle of the imaging surface. Imaging plates were exposed to ionizing radiation at a fixed distance using RXDC (MyRay, Italy) periapical x-ray source with 70 kV 8 mA 0.5 seconds as imaging parameters and scanned using VistaScan Mini Plus (Dürr Dental, Germany) device. Half of the imaging area after irradiation was placed in a hygienic sheath that was cut into half to protect the surface from the effect of the light to be applied. The irradiated plates were transported to the platform to stand for 1, 3, 5, and 10 minutes before scanning. During this delay, red, green, and blue lights were independently applied at varying intensities according to the PWM and LUX calibrations. At the end of the process, digital radiographs were obtained by scanning the plates at a theoretical resolution of approximately 40 lp/mm. As a result, six different regions were obtained in each image with half protected from LED light exposure and two-step alloy. Baseline images were obtained by keeping the plates in the dark before scanning. Digital radiographs were exported as 2514 x 3328 pixels in TIFF format and imported to the ImageJ software. In each of the six regions in the images Figure 3, three different ROIs with the size of 100 x 100 pixels each were determined randomly, and the MGVs were recorded as 0 representing pure black and 255 representing pure white. Imaging was repeated twice in all conditions.

Statistical Analysis

The characteristics of sensor readings were summarized by mean±standard deviation (SD), min-max and median (IQR: 1st quartile-3rd quartile), as MGV and contrast change were reported by median (IQR). The differences between various light flux settings within each time condition were examined by Kruskal-Wallis test with respect to the MGV of each region and contrast change between C and B regions. When necessary, the stepwise step-down method proposed by Campbell and Skillings was performed.[19] A p-value<0.05 was considered statistically significant. All statistical analyses were performed via IBM SPSS Statistics 22.0 software (IBM Corp. Released 2013. IBM SPSS Statistics for Windows, Version 22.0. Armonk, NY: IBM Corp.).

Results

The features of sensor readings are summarized in Table 1. Accordingly, the temperature was ranged between 27 °C and 31°C for PWM setup and 26 °C and 28 °C for LUX setup. The humidity was within range of 40-52% for PWM setup and 47-50% for LUX setup. In PWM setup, the mean LUX value was 44.71±0.93 in red color, 110.00±0.45 for green color and 84.35±0.49 for blue color. The distribution of the MGV measurements with PWM calibration is shown in Table 2. In A' region, after 1-, 3- and 5-minutes, the MGVs in all colors were significantly higher than the base image, and the difference among colors was significant (for all time conditions, p=0.015). The lowest MGVs were observed in red, green, and red colors at 1-, 3-, and 5-minutes, respectively. At 10-minutes, with green color, the digital radiograph is produced in half form without the light-exposed part of the plate, and the MGVs for the red and blue color were significantly higher than the base image and the difference among colors was significant (p=0.023). When the half-produced image at 10-minutes by green light exposure is excluded, the highest MGV was observed with blue color in all time conditions. In A region, after 1- and 3-minutes, the MGVs were significantly lower than the base image (p=0.023 and p=0.012, respectively), but the difference among colors was not significant (p>0.05). In 10-minutes, the MGVs were significantly higher than, equal to, and lower than the base image in the red, green, and blue colors, respectively, and the difference among colors was significant (p=0.012).

LUX values for calibrations were determined to be in the range of 43-44 LUX as a result of the analysis of the sensor readings in full PWM setup. PWM values in LUX setup were determined as 250, 100 and 135 for the red, green and the blue colors, respectively. The distribution of the MGV measurements with LUX calibration is shown in Table 3. In region A', at 1-minute, the MGVs of all colors were significantly higher than the base image, but the difference among colors was not significant (p=0.020). However, at 3-, 5-, and 10-minutes, the MGVs of all colors were significantly higher than the base image, and the difference among colors was significant (p=0.015). In all time delays, the lowest MGVs were obtained with the green color comparing the other colors. At 1-minute, the highest MGV was in the red color, while it was in the blue color at other delay times. In region A, the MGVs of all colors were significantly lower than those of base image at all times (for all times, p=0.012), but the difference among colors was not significant

Table 1. Descriptive statistics of the sensor readings

Setup Color	Descriptive Statistics	Temperature °C	Humidity %	Spectrum			LUX
				Infrared	Full	Visible	
PWM							
Red	Mean±SD	28.96±1.16	50.00±3.15	97.5±2.01	447.70±9.10	350.20±7.19	44.71±0.93
	Min-Max	27-31	40-52	92-104	428-488	335-384	42.79-49.31
	Median (IQR)	29 (28-29)	51 (51-51)	98 (97-99)	450 (444-454)	352 (347-355)	44.84 (44.31-45.30)
Green	Mean±SD	29.51±1.49	46.07±4.57	29.37±0.65	731.61±3.45	702.24±3.04	110.00±0.45
	Min-Max	27-31	40-52	28-30	720-736	691-707	108.23-110.84
	Median (IQR)	29 (28-31)	48 (40-51)	29 (29-30)	732 (731-734)	703 (701-704)	110.18 (109.71-110.35)
Blue	Mean±SD	29.09±0.74	48.06±2.13	6.01±0.21	528.79±3.12	522.78±3.07	84.35±0.49
	Min-Max	28-30	40-51	5-7	507-532	502-526	81.12-84.88
	Median (IQR)	29 (29-30)	49 (46-50)	6 (6-6)	530 (529-531)	524 (523-525)	84.55 (84.39-84.71)
LUX							
Red	Mean±SD	27.17±0.69	48.31±1.02	95.05±1.28	435.05±5.06	340.00±3.97	43.36±0.52
	Min-Max	26-28	47-50	91-99	422-462	331-363	42.27-46.55
	Median (IQR)	27 (27-28)	49 (47-49)	95 (94-96)	436 (433-438)	340 (338-342)	43.37 (43.06-43.68)
Green	Mean±SD	26.8±0.4	47.09±0.29	10.99±0.15	288.84±1.95	277.85±1.91	43.62±0.31
	Min-Max	26-27	47-48	10-12	282-292	272-281	42.66-44.13
	Median (IQR)	27 (27-27)	47 (47-47)	11 (11-11)	289 (288-290)	278 (277-279)	43.64 (43.48-43.81)
Blue	Mean±SD	27.52±0.5	47.75±0.43	2.99±0.09	273.71±1.51	270.71±1.50	43.70±0.25
	Min-Max	27-28	47-48	2-4	268-276	265-273	42.76-44.07
	Median (IQR)	28 (27-28)	48 (48-48)	3 (3-3)	274 (273-275)	271 (270-272)	43.74 (43.58-43.91)

SD: Standard deviation, Min: Minimum, Max: Maximum, IQR: 1st quartile-3rd quartile

(p>0.05). The MGV decreased evenly in all colors compared to the base image. In region B', at 1-minute, MGVs of all colors were significantly higher than those in the base images (p=0.025), while the difference among colors were not significant. The highest MGV was obtained in the red, while the lowest was in the green. At 3-minute, MGVs of all colors were significantly higher compared to the base image, and the MGV of the green color was significantly lower than the others (p=0.014). MGVs in red and blue colors reached to the maximum value. In B' and C' regions, in all colors, the MGVs at 5- and 10-minutes were significantly higher than the base images (p=0.013). All colors reached to the value of 254, and the differences among colors were not significant (p>0.05).

In Table 4, the contrast change is demonstrated with the difference in MGVs of the C-B and C'- B' regions. In none of the conditions, the contrast change in C-B regions were not significantly different than the base images (p>0.05). In PWM calibrations, at 1-minute, MGV differences of all colors were significantly lower than those of the base image (p=0.015), while the difference among colors were significant. The MGV difference was the highest in red (median: 7.36), followed by green (5.42), while the contrast is lost in blue color (0). In 3-minutes, all colors had significantly lower contrast than those of the base image (p=0.014), but the contrast in green color (5.02) was significantly higher than those of the other colors. The contrast was lost in red (0) and blue (0) colors. In 5-minutes, the contrast was lost (0) for all colors and significantly lower compared to the base image (p=0.013). At 10-minutes, when the half-image was excluded, contrast was lost in red (0) and blue (0) colors, and significantly lower than those of the base image (p=0.022). In LUX calibration, after 1-minute, the contrast of all colors was lower than those in the base image significantly (p=0.040), but the differences among colors were not significant. The highest contrast was observed in green, followed by blue, and the lowest in red color. In 3-minutes, the contrast was lost in red (0) and blue (0) colors, and contrast in green color (0.12) was significantly lower than the base image (p=0.014). In 5- and 10-minutes, the contrast was completely lost (0) in all colors compared to the base image (p=0.013), and the difference among colors was not significant.

Figure 1. Sensor readings are monitored through the serial port.

Discussion

In our study, the effects of the exposure to the three primary LED colors in delayed scanning of the PSP plates was evaluated in terms of signal loss and contrast change, by measuring the MGVs of six distinct regions in the digital images. In PWM setup, the signal loss in A' region was the highest for the blue color at 1-, 3- and 5-minutes. The lowest signal loss was observed in the red color at 1- and 5- minutes, and in the green color at 3-minutes. However, at 10-minutes, the half image was obtained as a result of signal loss in green color, while the same region was assigned to the MGV value of 255 with the blue color. Region A, in the half-produced image, was the only case in the study where MGV increased relative to the base image. As the half image was produced with green light at 10-minutes, MGV of the region A was increased in this unique radiograph. In LUX setup, the signal loss in A' region was the highest for the red color in the first minute, while the lowest in the green color. At all other times, the signal loss was the highest in the blue color, and the lowest in the green color. For contrast change, the difference in MGVs of the C-B and C'-B' regions were evaluated. Half of the PSP plate was protected from the light exposure, and the contrast change in C-B regions was not statistically significant. In PWM setup, at 1-minute, contrast change in C'-B' regions reduced to zero contrast in the blue color, and the lowest contrast loss was observed in red color. In 3-minutes, the contrast was lost for the blue and red colors; however, a contrast lower than the base image was obtained in green color. In LUX setup, at 1-minute, the contrast loss in C'-B' regions were higher in red color, followed by blue color; while in green color, a slight improvement in contrast was observed. At 3-minutes, a slight contrast remained only with the green color,

Table 2. Comparisons of each region's MGV between the enlightenment conditions for the calibration setup of 255 PWM.

Time		Regions					
	Color	A	B	C	A'	B'	C'
1 min							
	None	18 (18-18)[1]	237.27 (237.17-237.86)	246.64 (246.60-246.76)	18 (18-18)[1]	234.87 (233.89-235.92)[1]	245.92 (245.77-246.11)[1]
	Red	17 (17-17)[2]	237.58 (237.54-237.82)	247.33 (246.96-247.60)	89.11 (88.35-89.73)[2]	246.64 (246.27-247.10)[2]	254 (254-254)[2]
	Green	17 (16.98-17)[2]	237.66 (237.41-237.76)	247.61 (247.44-247.84)	117.27 (116.73-119.43)[3]	248.58 (248.38-249.50)[3]	254 (254-254)[2]
	Blue	17 (17-17)[2]	237.98 (237.82-238.03)	247.57 (247.57-247.83)	158.11 (158.08-159.45)[4]	254 (254-254)[4]	254 (254-254)[2]
	p-value	**0.023**	0.557	0.129	**0.015**	**0.015**	**0.013**
3 min							
	None	18 (18-18)[1]	237.93 (237.70-238.04)	247.24 (246.97-247.48)	18 (17.85-18)[1]	235.33 (234.30-235.52)[1]	246.11 (246.10-246.27)[1]
	Red	17 (17-17)[2]	237.68 (237.43-237.80)	247.34 (247.28-247.59)	189.27 (188.65-189.38)[2]	254 (254-254)[2]	254 (254-254)[2]
	Green	17 (17-17)[2]	237.07 (237.03-237.36)	247.22 (246.97-247.47)	118.90 (118.42-121.15)[3]	248.98 (248.76-249.55)[3]	254 (254-254)[2]
	Blue	17 (17-17)[2]	237.73 (237.68-237.81)	247.65 (247.41-247.79)	235.79 (235.50-236.17)[4]	254 (254-254)[2]	254 (254-254)[2]
	p-value	**0.012**	0.248	0.740	**0.015**	**0.014**	**0.013**
5 min							
	None	18 (18-18)[1]	237.77 (237.71-237.87)	247.13 (246.78-247.41)	18 (18-18)[1]	235.84 (234.81-236.13)[1]	246.45 (246.34-246.84)[1]
	Red	16 (16-16.01)[2]	237.41 (237.40-237.52)	247.36 (247.11-247.43)	222.82 (222.60-223.09)[2]	254 (254-254)[2]	254 (254-254)[2]
	Green	17 (17-17)[3]	238.61 (237.98-238.83)	248.12 (248.03-248.29)	237.63 (237.11-237.82)[3]	254 (254-254)[2]	254 (254-254)[2]
	Blue	17 (17-17)[3]	238.24 (237.78-238.26)	248.02 (247.54-248.12)	246.28 (246.26-246.55)[4]	254 (254-254)[2]	254 (254-254)[2]
	p-value	**0.012**	0.516	0.129	**0.015**	**0.013**	**0.013**
10 min							
	None	18 (18-18)[1]	237.9 (237.89-238.13)	247.47 (247.33-247.54)	18 (17.82-18)[1]	236.21 (235.06-236.57)[1]	246.73 (246.57-246.84)[1]
	Red	16 (16-16)[2]	238.04 (237.85-238.38)	247.59 (247.48-247.84)	243.20 (243.10-243.41)[2]	254 (254-254)[2]	254 (254-254)[2]
	Green	19 (19-19)[3]	238.40 (238.31-238.56)	248.10 (248.05-248.1)	–	–	–
	Blue	18 (18-18)[1]	238.41 (238.33-238.61)	247.92 (247.86-248.22)	255 (255-255)[3]	255 (255-255)[3]	255 (255-255)[3]
	p-value	**0.012**	0.270	0.092	**0.023**	**0.021**	**0.021**

Signal loss is reported by median (IQR). [1,2,3,4] : Each number represents a homogeneous subset.

Figure 2. The developed system ready to emit green light to the half of the active surface of the PSP. The front door is opened for visualization of the electronical units in the photo.

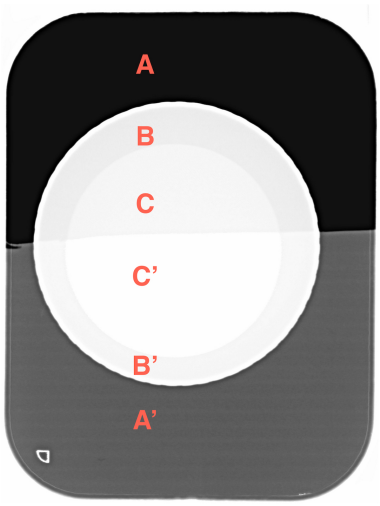

Figure 3. As half of the active surface is protected from the exposure of light, in total, 6 distinct regions are obtained in each image.

while after 5-minutes, the contrast was lost in all colors.

The dynamic range of a radiography system is the latitude of x-ray exposure, which results in diagnostically acceptable images. The digital systems offer a much broader dynamic range than the analog systems; thus, high quality digital images can be produced with a much lower x-ray dose when compared to analog systems. Also, in digital systems, the irradiation remaining below and above the optimal level can be compensated to a level, reducing the need for repeated exposures.[7,20] Berkhout et al. compared the exposure range of five intraoral radiography systems (two SS systems, two PSP systems and film) with variable exposure times. The obtained images were rated by seven observers, as diagnostically acceptable and preferred radiographs. The authors reported that all digital systems require less exposure than the film for diagnostically acceptable radiographs, while the dose for the preferred radiographs is reduced only in SS systems. In SS sensors, over-exposure may lead to artifacts such as blooming. Reduce in image quality as the dose increase can be an indicator for over-exposure, however, severe artifacts may require re-takes. In PSP systems, the dynamic range is reported to be wider, but the dose required for the preferred radiographs is ten times higher than the minimal acceptable dose. This compensation in over-exposure may prevent the need for repetitions but may also result in adopting higher doses without any sign.[20] Marinho-Vieira et al. assessed the dynamic range and enhancement ability of radiographs using five intraoral digital radiographic systems (two SS sensors and three PSP plates) as image receptors. The digital sensors were irradiated for 10 distinct exposure times, and the PSP systems were reported to provide a broader dynamic range.[7] Galvão defined automatic exposure compensation (AEC) as "a non-linear enhancement of the image histogram that detects the lowest and highest pixel values and modifies the greyscale to increase image contrast".[21] Presence of high-density dental materials is suggested as a factor influencing the overall grey

Table 3. Comparisons of each region's MGV between the enlightenment conditions for the calibration setup of LUX.

Time		Regions					
	Color	A	B	C	A'	B'	C'
1 min							
	None	18 (18-18)[1]	237.27 (237.17-237.86)	246.64 (246.60-246.76)[1]	18 (18-18)[1]	234.87 (233.89-235.92)[1]	245.92 (245.77-246.11)[1]
	Red	17 (17-17)[2]	237.34 (237.21-237.47)	247.08 (246.92-247.30)[1]	92.97 (92.77-94.09)[2]	247.14 (246.60-247.26)[2]	254 (254-254)[2]
	Green	17 (17-17)[2]	237.83 (237.57-237.89)	247.03 (246.93-247.37)[1]	35.77 (35.36-36.97)[2]	243.41 (242.78-243.70)[2]	253.81 (253.79-253.90)[2]
	Blue	17 (17-17)[2]	237.52 (237.34-237.55)	246.31 (246.31-246.35)[2]	90.55 (89.60-92.61)[2]	246.42 (246.24-247.30)[2]	254 (254-254)[2]
	p-value	**0.012**	0.691	**0.043**	**0.020**	**0.025**	**0.024**
3 min							
	None	18 (18-18)[1]	237.93 (237.70-238.04)	247.24 (246.97-247.48)	18 (17.85-18)[1]	235.33 (234.30-235.52)[1]	246.11 (246.10-246.27)[1]
	Red	17 (17-17)[2]	237.91 (237.79-238.05)	246.99 (246.79-247.36)	190.28 (189.70-190.66)[2]	254 (254-254)[2]	254 (254-254)[2]
	Green	17 (17-17)[2]	237.78 (237.71-237.87)	247.34 (247.22-247.58)	133.23 (132.45-135.67)[3]	253.89 (252.60-253.92)[3]	254 (254-254)[2]
	Blue	17 (17-17)[2]	237.37 (237.16-237.73)	246.76 (246.58-246.81)	198.56 (198.21-199.85)[4]	254 (254-254)[2]	254 (254-254)[2]
	p-value	**0.012**	0.622	**0.238**	**0.015**	**0.014**	**0.013**
5 min							
	None	18 (18-18)[1]	237.77 (237.71-237.87)	247.13 (246.78-247.41)	18 (18-18)[1]	235.84 (234.81-236.13)[1]	246.45 (246.34-246.84)[1]
	Red	17 (17-17)[2]	237.94 (237.66-238.17)	247.45 (247.35-247.59)	220.75 (220.26-220.75)[2]	254 (254-254)[2]	254 (254-254)[2]
	Green	17 (17-17)[2]	237.73 (237.57-237.87)	247.28 (247.19-247.52)	181.32 (180.63-182.99)[3]	254 (254-254)[2]	254 (254-254)[2]
	Blue	17 (17-17)[2]	237.78 (237.75-238.07)	247.38 (246.87-247.47)	228.88 (228.84-229.72)[4]	254 (254-254)[2]	254 (254-254)[2]
	p-value	**0.012**	0.933	0.789	**0.015**	**0.013**	**0.013**
10 min							
	None	18 (18-18)[1]	237.90 (237.89-238.13)	247.47 (247.33-247.54)	18 (17.82-18)[1]	236.21 (235.06-236.57)[1]	246.73 (246.57-246.84)[1]
	Red	17 (17-17)[2]	237.83 (237.72-237.92)	247.67 (247.65-247.79)	243.05 (242.98-243.17)[2]	254 (254-254)[2]	254 (254-254)[2]
	Green	17 (17-17)[2]	238.10 (237.96-238.38)	247.39 (247.32-247.71)	227.94 (227.66-228.51)[3]	254 (254-254)[2]	254 (254-254)[2]
	Blue	17 (17-17)[2]	238.46 (238.41-238.48)	247.94 (247.91-248.14)	246.03 (245.95-246.12)[4]	254 (254-254)[2]	254 (254-254)[2]
	p-value	**0.012**	0.147	0.132	**0.015**	**0.013**	**0.013**

Signal loss is reported by median (IQR). [1,2,3,4] : Each number represents a homogeneous subset.

Table 4. Comparisons of contrast change between the enlightenment conditions within each calibration method

Time		PWM		LUX	
	Color	C-B	C'- B'	C-B	C'- B'
1 min					
	None	9.28 (8.85-9.43)	11.05 (10.19-11.88)[1]	9.28 (8.85-9.43)	11.05 (10.19-11.88)[1]
	Red	9.75 (9.41-9.78)	7.36 (6.90-7.73)[2]	9.48 (9.45-9.96)	6.86 (6.74-7.4)[2]
	Green	10.09 (9.92-10.25)	5.42 (4.50-5.62)[3]	9.71 (9.36-9.74)	10.60 (10.21-11.11)[1,2]
	Blue	9.59 (9.54-10.01)	0 (0-0)[4]	8.79 (8.76-9.01)	7.59 (6.70-7.76)[1,2]
	p-value	0.164	0.015	0.183	0.040
3 min					
	None	9.24 (9.17-9.52)	10.79 (10.75-11.81)[1]	9.24 (9.17-9.52)	10.79 (10.75-11.81)[1]
	Red	9.55 (9.48-10.10)	0 (0-0)[2]	9.32 (8.99-9.44)	0 (0-0)[2]
	Green	9.66 (9.61-10.19)	5.02 (4.45-5.24)[3]	9.37 (9.35-9.77)	0.12 (0.08-1.40)[3]
	Blue	9.76 (9.60-10.02)	0 (0-0)[2]	9.02 (8.85-9.47)	0 (0-0)[2]
	p-value	0.497	0.014	0.668	0.014
5 min					
	None	9.17 (8.92-9.61)	10.81 (10.60-11.74)[1]	9.17 (8.92-9.61)	10.81 (10.60-11.74)[1]
	Red	9.72 (9.58-9.92)	0 (0-0)[2]	9.51 (9.42-9.69)	0 (0-0)[2]
	Green	9.33 (9.20-10.22)	0 (0-0)[2]	9.38 (9.32-9.87)	0 (0-0)[2]
	Blue	9.78 (9.28-10.34)	0 (0-0)[2]	9.20 (8.88-9.43)	0 (0-0)[2]
	p-value	0.764	0.013	0.546	0.013
10 min					
	None	9.30 (9.28-9.44)	10.74 (10.27-11.63)[1]	9.30 (9.28-9.44)	10.74 (10.27-11.63)[1]
	Red	9.55 (9.10-9.99)	0 (0-0)[2]	10.02 (9.84-10.04)	0 (0-0)[2]
	Green	–	–	9.29 (8.94-9.75)	0 (0-0)[2]
	Blue	9.68 (9.33-9.89)	0 (0-0)[2]	9.58 (9.48-9.73)	0 (0-0)[2]
	p-value	0.740	0.022	0.270	0.013

Contrast is reported by median (IQR). [1,2,3,4] : Each number represents a homogeneous subset.

values and the image contrast.[21–23] In our study, half of the surface of the PSP plates were protected from the LED light exposure. Thus, it was aimed to evaluate the dynamic range and AEC. Lumen is the total amount of light emitted from a source. LUX is the unit for defining the amount of light in the certain area on a surface.[24] In our study, while three primary colors of light were produced by an RGB LED, the illumination on the ground was monitored with the TSL2591 sensor. The PWM value determines how long the RGB LED will be on or off during a duty cycle. Thus, as the PWM is increased, the total amount of light emitted from the source increases, while the opposite happens when it decreases. The light intensity on the floor is converted into a digital signal by TSL2591 sensor, which combines one broadband photodiode (visible plus infrared) and one infrared-responding photodiode on a single CMOS integrated circuit. The irradiance measured on each photodiode are converted to digital using two integrating analog-to-digital converters, and the difference in both values represents the visible light. Ambient light can be monitored in LUX using an empirical formula.

According to the datasheet of the TSL2591 sensor, spectral responsivity of the sensor is in the range of 400-1100 nm and approximated to the human eye response. As recognized by the Commission Internationale de l'Éclairage (CIE), the human eye can see in the range of 400-700 nm, with a perception of brightness that varies with color. Bright vision is best at 555 nm, while the dim vision is best at 505 nm.[24] In our study, intermediate colors were not used due to their subjective nature. As only the primary colors were used at full PWM, different LUX values were measured on the floor. This can suggest that the maximum output from the light source is different for each color, according to the LUX measurements. In sensor readings, SDs were found to be higher in red color. This can be related to the spectral response curve of the sensor.

In this study, the Arduino-based system is developed with the sensors available in the market at a reasonable price. The lack of calibrated measurements with industry-level devices is a limitation of our study. However, the purpose of establishing this embedded system is to provide standardization between different light conditions. Therefore, it can be suggested that the lack of calibration of sensor data such as LUX or temperature will not prevent the comparison of the effect of exposure to light colors, as the changes are monitored precisely. Also, the readings of the TSL2591 sensor are optimized to the human color perception, which the perceived brightness varies with the wavelength of the light. In future studies, an advanced light spectroscopy sensor such as AS7265x can be used for calculating the amount of light independent of human perception and equalizing the amount of light in different colors.

Conclusion

In fixed LUX, the signal loss is lowest in green colors in all delays, except at 1-minute, and highest in blue color. Contrast loss in green color was the lowest. According to the results of this study, effect of the green ambient light might be lower than the red and the blue colors.

Financial support

The authors declare that any financial support was not received.

Author Contributions

H.A. and K.O. conceived the ideas; H.A. and A.A. collected and analyzed the data; K.O., H.A. and A.A. led the writing.

Conflict of Interest

Authors declare that there is no conflict of interest.

Acknowledgements

The 3D manufactured platform is designed, produced, and combined in Cerrahpaşa Research, Simulation and Design Center (CAST). This research will be presented in the 4th International Congress of Oral Diagnosis and Maxillofacial Radiology which will be held in Palm Wings Ephesus Hotel, Selçuk-İzmir on October 19-23, 2022.

Authors' ORCID(s)

H.A. 0000-0001-7400-9938
K.O. 0000-0001-6768-0176
A.A. 0000-0002-9734-4138

References

1. Brennan J. An introduction to digital radiography in dentistry. J Orthod. 2002;29(1):66–9. Available from: https://www.ncbi.nlm.nih.gov/pubmed/11907314. doi:10.1093/ortho/29.1.66.
2. Mallya S, Lam E. White and Pharoah's Oral Radiology Principles and Interpretation. 8th ed. United States: Mosby; 2018.
3. Noorsaeed AS, Almohammedsaleh AH, Alhayek MM, Alnajar AA, Kariri ON, Albakri AIM, et al. Overview on Updates on Digital Dental Radiography. Journal of Pharmaceutical Research International. 2021;33(59B):23–28. doi:10.9734/jpri/2021/v33i59B34347.
4. Hassan S, Bhateja S, Arora G, Prathyusha F. Digital Radiography. Int J Maxillofac Imaging. 2020;6:33–36. doi:10.18231/j.ijmi.2020.009.
5. Kaur J, Parganiha Y, Dubey V, Singh D. A review report on medical imaging phosphors. Res Chem Intermed. 2014;40:2837–2858. doi:http://dx.doi.org/10.1007/s11164-013-1132-1.
6. Parks ET, Williamson GF. Digital radiography: an overview. J Contemp Dent Pract. 2002;3(4):23–39. Available from: https://www.ncbi.nlm.nih.gov/pubmed/12444400.
7. Marinho-Vieira LE, Martins LAC, Freitas DQ, Haiter-Neto F, Oliveira ML. Revisiting dynamic range and image enhancement ability of contemporary digital radiographic systems. Dentomaxillofac Radiol. 2022;51(4):20210404. Available from: https://www.ncbi.nlm.nih.gov/pubmed/34860568. doi:10.1259/dmfr.20210404.
8. Kondaveeti HK, Kumaravelu NK, Vanambathina SD, Mathe SE, Vappangi S. A Systematic Literature Review on Prototyping with Arduino: Applications, Challenges, Advantages, and Limitations. Comput Sci Rev. 2021;40(C). Available from: https://doi.org/10.1016/j.cosrev.2021.100364. doi:10.1016/j.cosrev.2021.100364.
9. El-Abd M. A Review of Embedded Systems Education in the Arduino Age: Lessons Learned and Future Directions. Int J Eng Pedagog. 2017;7(2):79–93. Available from: https://doi.org/10.3991/ijep.v7i2.6845. doi:10.3991/ijep.v7i2.6845.
10. Nayyar A, Puri V. A review of Arduino board's, Lilypad's & Arduino shields. 2016 3rd International Conference on Computing for Sustainable Global Development (INDIACom). 2016:1485–1492.
11. Lin L, Fang Y, Liao Y, Chen G, Gao C, Zhu P. 3D Printing and Digital Processing Techniques in Dentistry: A Review of Literature. Adv Eng Mater. 2019;21(6):1801013. Available from: https://onlinelibrary.wiley.com/doi/abs/10.1002/adem.201801013. doi:https://doi.org/10.1002/adem.201801013.

12. Zaharia C, Gabor A, Gavrilovici AM, Stan A, Idorasi L, Sinescu C, et al. Digital Dentistry — 3D Printing Applications. J Interdiscip Med. 2017;2. doi:10.1515/jim-2017-0032.
13. Prasad S, Kader NA, Sujatha G, Raj T, Patil S. 3D printing in dentistry. J 3D print med. 2018;2(3):89–91. Available from: https://www.futuremedicine.com/doi/abs/10.2217/3dp-2018-0012. doi:10.2217/3dp-2018-0012.
14. MacDonald E, Salas R, Espalin D, Perez MA, Aguilera E, Muse D, et al. 3D Printing for the Rapid Prototyping of Structural Electronics. IEEE Access. 2014;2:234–242. doi:https://doi.org/10.1109/ACCESS.2014.2311810.
15. Vinodh S, Sundararaj GK, Devadasan SR, Kuttalingam D, Rajanayagam D. Agility through rapid prototyping technology in a manufacturing environment using a 3D printer. J Manuf Technol Manag. 2009;20:1023–1041. doi:https://doi.org/10.1108/17410380910984267.
16. Tashiro M, Nakatani A, Sugiura K, Nakayama E. Analysis of image defects in digital intraoral radiography based on photostimulable phosphor plates. Oral Radiol. 2022. doi:10.1007/s11282-022-00645-8.
17. Akdeniz BG, Gröndahl HG, Kose T. Effect of delayed scanning of storage phosphor plates. Oral Surg Oral Med Oral Pathol Oral Radiol Endod. 2005;99(5):603–7. doi:10.1016/j.tripleo.2004.10.021.
18. Eskandarloo A, Yousefi A, Soheili S, Ghazikhanloo K, Amini P, Mohammadpoor H. Evaluation of the Effect of Light and Scanning Time Delay on The Image Quality of Intra Oral Photostimulable Phosphor Plates. Open Dent J. 2017;11:690–700. doi:10.2174/1874210601711010690.
19. Campbell G, Skillings JH. Nonparametric Stepwise Multiple Comparison Procedures. J Am Stat Assoc. 1985;80(392):998–1003. Available from: https://www.tandfonline.com/doi/abs/10.1080/01621459.1985.10478216. doi:10.1080/01621459.1985.10478216.
20. Berkhout WE, Beuger DA, Sanderink GC, van der Stelt PF. The dynamic range of digital radiographic systems: dose reduction or risk of overexposure? Dentomaxillofac Radiol. 2004;33(1):1–5. doi:10.1259/dmfr/40677472.
21. Galvão NS, Nascimento EHL, Lima CAS, Freitas DQ, Haiter-Neto F, Oliveira ML. Can a high-density dental material affect the automatic exposure compensation of digital radiographic images? Dentomaxillofac Radiol. 2019;48(3):20180331. doi:10.1259/dmfr.20180331.
22. Dashpuntsag O, Yoshida M, Kasai R, Maeda N, Hosoki H, Honda E. Numerical Evaluation of Image Contrast for Thicker and Thinner Objects among Current Intraoral Digital Imaging Systems. Biomed Res Int. 2017;2017:5215413. Available from: https://doi.org/10.1155/2017/5215413. doi:10.1155/2017/5215413.
23. Maciel ERC, Nascimento EHL, Gaêta-Araujo H, Pontual M, Pontual ADA, Ramos-Perez FMM. Automatic exposure compensation in intraoral digital radiography: effect on the gray values of dental tissues. BMC Med Imaging. 2022;22(1):4. doi:10.1186/s12880-021-00733-x.
24. Bushong SC. Radiologic Science for Technologists: Physics, Biology, and Protection. 10th ed. St. Louis: Mosby; 2013.